

**2007 American WJTA Conference and Expo  
August 19-21, 2007 • Houston, Texas**

Paper

**HIGH-SPEED OBSERVATIONS OF SUBMERGED WATER JETS  
ISSUING FROM AN ABRASIVE WATER JET NOZZLE**

S. Shimizu  
College of Engineering, Nihon University  
Koriyama, Japan

H. Adachi, K. Izumi  
Hitachi, Ltd. Power Systems, Hitachi Works  
Hitachi, Japan

H. Sakai  
Sugino Machine Ltd. Plant Equipment Production Department, Design Section  
Namerikawa, Japan

**ABSTRACT**

In order to clarify the flow structure of abrasive water injection jets (AWIJs) under a submerged environment, high-speed observations of water jets issuing from an AWIJ nozzle are conducted using high-speed video. The injection pressure of the jet is in the range of from 100 to 380 MPa. The submergence is approximately 1 m. The airflow rates supplied from the abrasive port of the AWIJ nozzle are 0, 20, and 50 NL/min, but abrasive particles are not contained in the airflow. High-speed videos are taken at a frame rate of 87,600 frames per second. The unsteady characteristics of cavitating jets and ventilated jets are discussed in the paper.

## 1. INTRODUCTION

In the last quarter century, abrasive water jets (AWJs) have been established as a cutting technique for industrial machining. Abrasive water jets can be categorized into abrasive water injection jets (AWIJs) and abrasive water suspension jets (AWSJs) based on the generation mechanism and the phase composition.<sup>(1)</sup> An AWIJ consists of solid particles, air, and water, and is considered to be a three-phase jet flow. In contrast, an AWSJ consists of solid particles and water, and is considered to be a two-phase jet flow. The structure and cutting capability of AWJs differ markedly according to the environment around the jets and the phase composition of the jets. Abrasive water jets are widely used in air for practical applications, and the structure and drilling and cutting capability of AWJs in air have been studied extensively.<sup>(1,2)</sup> However, studies on AWJs in submerged environments are relatively few. Haferkamp, Louis, and Meier<sup>(3,4)</sup> studied the cutting capability of AWIJs under submerged environments experimentally. Shimizu et al.<sup>(5)</sup> conducted drilling tests by submerged AWSJs at the injection pressure of 12 MPa. The cutting potential of submerged AWSJs at the injection pressure of 140 MPa was reported by Hung et al.<sup>(6)</sup> In addition, both AWIJs and AWSJs, are applicable to drilling and cutting in submerged environments, but the cutting capability of the jets decreases dramatically with the increase of distance between the nozzle and the work-piece.

Unsteady behavior of submerged water jets has been studied extensively<sup>(7-11)</sup> from the standpoint of cavitation erosion by high-speed cavitating jets. In order to improve the distance over which the submerged jet would retain an effective pressure, air shrouded water jets were investigated, and the effective reach of a submerged water jet was found to increase when a concentric air shroud was supplied around the water jet.<sup>(12,13)</sup> For submerged applications of AWIJs, an abrasive cutting head with an air mantled nozzle<sup>(3,14)</sup> was proposed. However, the flow structures of AWJs under submerged environments have not been clarified sufficiently.

In the present investigation, high-speed observations of a submerged water jet issuing from an AWIJ nozzle are conducted at the injection pressure range of from 100 to 380 MPa with and without air supply. Abrasive particles are not contained in the airflow when air is supplied from the abrasive port of the AWIJ nozzle head. The unsteady characteristics of the cavitating jets and the ventilated jets are discussed in order to understand the cutting capability of submerged AWJs.

## 2. EXPERIMENTAL APPARATUS AND CONDITIONS

Observations of the jets are conducted using a rectangular water tank. The tank is 2 m in length, 1.5 m in width, and 2 m in height. The jet is supplied from an intensifier pump through an abrasive water injection jet (AWIJ) nozzle head at the injection pressure range of from 100 to 380 MPa. The jet discharges horizontally into the water tank. The depth of water at the nozzle position is approximately 0.95 m and is maintained constant during the experiments. The dimensions of the AWIJ nozzle head are as follows:

Diameter of water jet orifice;	0.62 mm
Diameter of focusing nozzle;	1.5 mm
Length of focusing nozzle;	76.2 mm

Air is supplied from the abrasive port of the AWIJ nozzle head, but abrasive particles are not contained in the airflow. The observations of the jets are conducted at the airflow rates of 0, 20, and 50 NL/min.

The submerged water jets are observed using a high-speed video camera, Photron Fast Cam-Max 120 K, at a frame rate of 87,600 frames per second. Photron Fastcam Viewer is used for image processing.

The parameter of similitude in cavitation is defined by the cavitation number  $\sigma$  as follows:

$$\sigma = (p_a - p_v) / (p_i - p_a) \quad (1)$$

where  $p_a$ ,  $p_i$ , and  $p_v$  are the ambient pressure, the injection pressure, and the vapor pressure of water, respectively. The cavitation numbers under the present experimental conditions are listed in Table 1.

### 3. EXPERIMENTAL RESULTS AND DISCUSSION

Observations of the submerged water jets issuing from the AWIJ nozzle head without air supply are conducted at the injection pressure range of from 100 to 380 MPa. Since pneumatic transport drags the abrasive particles into the mixing chamber of the AWIJ nozzle head, the water jets issuing from the AWIJ nozzle head without air supply appear to be unrealistic. This flow condition is considered to be as follows. When a solid particle moves in a stationary fluid, the solid particle decelerates faster in the liquid phase than in the gas phase. Accordingly, the submerged water jet issuing from the AWIJ nozzle head without air supply is the most difficult flow condition in which to sustain the velocity of the abrasive particle in the jet if abrasive particle exists in the jet. From another point of view, the submerged jet issuing from the AWIJ nozzle head without air supply is considered to correspond to the flow issuing from a sheathed AWSJ nozzle<sup>(15)</sup> in a submerged environment.

Figure 1 shows a series of photographs of a submerged jet issuing from the AWIJ nozzle head without air supply at the injection pressure  $p_i$  of 100 MPa. High-speed videos are taken at a frame rate of 87,600 frames per second for approximately 0.114 s up to 10,000 frames. Frame numbers are indicated on the left side of each photograph. The flow direction is left to right. In the following photographs, the right end of each photograph corresponds to approximately 98 mm from the exit of the focusing nozzle. The standoff distance  $X$  is defined as the axial distance measured from the focusing nozzle exit. The cavitation is seen as white clouds. At frame number 2,150, the cavitation cloud issuing from the focusing nozzle spreads radially just downstream from the focusing nozzle exit. As time proceeds, the cavitation cloud moves downstream, and a tongue-like cloud protrudes in the downstream direction from the cavitation cloud.

Another series of photographs of the jet at  $p_i = 100$  MPa without air supply is shown in Fig. 2. With the movement of a tongue-like cloud, the cavitation cloud downstream of the tongue-like cloud shrinks, and a cavitation free concave region is observed between the tongue-like cloud

and the downstream cavitation cloud, which suggests the existence of a high-pressure region downstream of the tongue-like cloud.

Rapid growth of a cavitation cloud can occasionally be observed. The rapid growth of a cavitation cloud is completely different from the abovementioned protrusion of a tongue-like cloud. Figure 3 shows a series of photographs of the jet at  $p_i = 100$  MPa without air supply. Between frame numbers 2,324 and 2,325, the downstream end of the cavitation cloud issuing from the focusing nozzle extends abruptly. The velocity of the cavitation cloud is calculated to be approximately 700 m/s if the extension of the cavitation cloud occurs within 11.4  $\mu$ s, one frame of the high-speed video. In the case of rapid extension of the cavitation cloud, the boundary of the cavitation cloud is rather unclear compared with the tongue-like cavitation clouds shown in Figs. 1 and 2. The rapid extension of the cavitation cloud is considered to be caused by passing of an expansion wave.

A series of photographs at  $p_i = 300$  MPa without air supply is shown in Fig. 4. Since the jet near the focusing nozzle exit is illuminated from behind, the cavitation clouds appear black. A thin cavitation cloud issuing from the focusing nozzle is connected with an elliptic cavitation cloud, which is considered to be vortex ring cavitation around the jet. The elliptic cavitation cloud shrinks until frame number 6,806 and then expands again. The cavitation cloud upstream of the elliptic cloud is constricted in frame numbers 6,810 to 6,814, and the cavitation cloud issuing from the focusing nozzle breaks off at approximately  $X = 20$  mm in frame number 6,818.

The downstream end position of the tongue-like cloud is measured at every four or five frames according to the injection pressure: every five frames for  $p_i = 100$  MPa and every four frames for  $p_i = 200$  MPa. From these data, protruding velocities of tongue-like clouds are calculated for the jets at  $p_i = 100$  and 200 MPa without air supply. The protruding velocity  $V$  is normalized by the theoretical jet velocity  $V_{th}$  defined as follows:

$$V_{th} = (2 p_i / \rho)^{1/2} \quad (2)$$

Examples of the calculated protruding velocity  $V/V_{th}$  with respect to the position of the downstream end of the tongue-like cloud  $X$  are shown in Fig. 5. The black circles shown in Fig. 5 represent the  $V/V_{th}$  of the tongue-like cloud shown in Fig. 1. The protruding velocity of the cloud  $V/V_{th}$  at approximately  $X = 30$  mm is relatively large at approximately 0.4 but decreases with the standoff distance  $X$ . However,  $V/V_{th}$  increases abruptly at approximately  $X = 60$  mm. The photographs of frame numbers 2,167 and 2,168 shown in Fig. 1 correspond to the tongue-like cloud at  $X = 60$  mm. When  $V/V_{th}$  is relatively large, the downstream end of the tongue-like cloud is sharp, and then becomes rounded. In addition,  $V/V_{th}$  decreases with the increase in  $X$ . The above mentioned tongue-like cavitation cloud is considered to occur in the region of high shear at the boundary between the surrounding fluid and the high-speed jet flow that penetrates the upstream bubbly zone. Another example of  $V/V_{th}$  is shown in Fig. 5 by black triangles. The protruding velocity  $V/V_{th}$  reaches a maximum at approximately  $X = 55$  mm.

The distribution of  $V/V_{th}$  with  $X$  is shown in Fig. 6 for the injection pressures of 100 and 200 MPa without air supply. The numbers of data at  $p_i = 100$  and 200 MPa are 139 and 77,

respectively. The average values of  $V/V_{th}$  are 0.29 for  $p_i = 100$  MPa and 0.30 for  $p_i = 200$  MPa. The maximum  $V/V_{th}$  is approximately 0.5 for both cases. In Fig. 6, the boundaries of the existing region of  $V/V_{th}$  for  $p_i = 100$  and 200 MPa are indicated by solid lines and dotted lines, respectively. When  $X$  is large, the upper boundary of  $V/V_{th}$  for  $p_i = 200$  MPa becomes larger than that for  $p_i = 100$  MPa. When the injection pressure is large, the cavitation number becomes smaller, as shown in Table 1, and cavitation occurs more violently around the jet. Since the tongue-like cavitation cloud is considered to occur in the region of high shear at the boundary between the surrounding fluid and the high-speed jet flow that penetrates the upstream bubbly zone, Figure 6 suggests that cavitation around the jet suppresses the deceleration of the jet velocity.

Series of photographs of submerged jets issuing from the AWIJ nozzle with air supply at  $p_i = 300$  MPa are shown in Figs. 7 and 8. The airflow rates are 20 and 50 NL/min. Since the unsteadiness of the flow is suppressed drastically by the ventilation, the photographs are shown at every ten frames.

The time variations of the boundaries of cavitation clouds or ventilated cavity clouds at  $X = 10$  mm are obtained by the high-speed video for approximately 0.0584 s. Figures 9 to 11 and 12 to 14 show the results for  $p_i = 100$  and 300 MPa, respectively. The airflow rates are 0, 20, and 50 NL/min. When the air flow rate is zero, cavitation clouds that are considered to result from vortex ring cavitation are formed periodically in the region near the focusing nozzle exit, as shown in Figs. 1 and 4, and the boundaries of the cavitation clouds change drastically.

The frequencies of time variations of cavitation cloud diameter in the region near the focusing nozzle exit are obtained in order to study the unsteady behavior of the cavitation cloud. Figure 15 shows the frequency of the time variation of cavitation cloud diameter with respect to the injection pressure at  $X = 10$  mm. As pointed out by Yamauch et al.,<sup>(9)</sup> the discharge frequency of the vortex ring cavitation decreases with the decrease of the cavitation number, or, in this case, the increase of the injection pressure. Kobayashi et al.<sup>(11)</sup> studied the unsteady behavior of the cavity boundary of a jet issuing from an ordinary convergent nozzle at the injection pressure of 30 MPa and reported that the occurrence frequency of vortex ring cavitation in the region near the nozzle exit was 1.8 or 2.2 kHz. If we extrapolate the present results, the frequency at  $p_i = 30$  MPa is approximately 2 kHz. This value roughly corresponds to the result reported by Kobayashi et al.

When air is supplied from the abrasive port of the AWIJ nozzle, the steadiness of the jet improved remarkably, and the amplitude of the time variations of the ventilated cavity diameter near the focusing nozzle exit becomes smaller, as shown in Figs. 9 to 14. Figure 16 shows the average diameter of the cavity cloud with respect to the air flow rate  $Q_{air}$  at  $X = 10$  mm for the injection pressures of 100, 200, 300, and 380 MPa. When  $p_i = 100$  and 200 MPa, the average cavity diameter reaches the minimum at approximately  $Q_{air} = 20$  NL/min. However, the cavity diameters for  $p_i = 300$  and 380 MPa decrease with the increase in the airflow rate, within limits.

In order to investigate the unsteady behavior of the cavitation clouds and the ventilated cavity clouds in a large standoff distance region, the time variations of the gray level of the images of the high-speed video on the jet axis at  $X = 70, 80,$  and  $90$  mm are obtained for approximately

6.85 ms at the injection pressure of  $p_i = 100$  MPa. In the present high-speed video, a gray level of 0 corresponds to black, and a gray level of 255 corresponds to white. Since the jet at  $p_i = 100$  MPa is illuminated by reflected light, the gray level of the reference pixel takes a larger value when a cavity cloud passes the reference pixel. The time variations of the gray level normalized by the maximum level 255 are shown in Figs. 17 to 19 for  $Q_{air} = 0, 20, \text{ and } 50$  NL/min, respectively. When an air supply is not provided, the gray levels change greatly with time. Since cavitation clouds move downstream accompanying collapse and rebound, peaks of the gray levels at  $X = 70, 80, \text{ and } 90$  mm do not always correspond to each other. In the case of  $Q_{air} = 20$  NL/min, the peaks of the gray level at  $X = 70, 80, \text{ and } 90$  mm correspond clearly to each other, since the transfer of ventilated cavity clouds dominates this phenomenon. When  $Q_{air} = 50$  NL/min, the amplitude of the gray level becomes smaller and the periodic time becomes longer compared with that of  $Q_{air} = 20$  NL/min. In the region just downstream of the focusing nozzle exit, the steadiness of the flow is improved by the ventilation at the airflow rate of  $Q_{air} = 20$  NL/min, as shown in Fig. 10. However, the steadiness of the flow in a large standoff distance region is improved by the ventilation at larger airflow rates.

#### 4. CONCLUSIONS

High-speed observations of a submerged water jet issuing from an AWIJ nozzle head were conducted at the injection pressure range of from 100 to 380 MPa with and without air supply. Abrasive particles were not contained in the airflow when air was supplied from the abrasive port of the AWIJ nozzle head. The unsteady behavior of the jets with and without air supply was discussed. Main specific points of interest are as follows:

- (1) The cavitation cloud around the jet is extremely unsteady. Even if the cavitation number is lower than 0.001, the cavitation cloud sometimes breaks off just downstream of the focusing nozzle exit.
- (2) Vortex ring cavitation occurs around the jet in the region just downstream of the focusing nozzle exit. The frequency of occurrence decreases with the increase of the injection pressure. When the injection pressure is 100 to 380 MPa, the occurring frequency is 1.5 to 1.8 kHz in the present experiments.
- (3) Protrusion of a tongue-like cavitation cloud, which is considered to occur in the region of high shear at the boundary between the surrounding fluid and the high-speed jet flow that penetrates the upstream bubbly zone, is frequently observed. The maximum protrusion velocity and the average protrusion velocity of the tongue-like cavitation cloud normalized by the theoretical jet velocity are approximately 0.5 and 0.3, respectively. When the cavitation number is small, a larger protrusion velocity tends to persist to a larger standoff distance region.
- (4) When air is supplied from the abrasive port of the AWIJ nozzle, the steadiness of the flow is improved remarkably.
- (5) The ventilated jet flow in the region just downstream of the focusing nozzle exit becomes steady at the optimum airflow rate. The optimum airflow rate tends to increase with the increase of the injection pressure.
- (6) The jet flow in the region far from the focusing nozzle exit becomes steady when air is supplied at a flow rate larger than the abovementioned optimum air flow rate

## 5. ACKNOWLEDGEMENTS

The authors would like to thank Mr. M. Kono and Mr. Y. Omori for their help in carrying out the image processing of the high-speed videos.

## 6. REFERENCES

- (1) A. W. Momber and R. Kovacevic, Principles of abrasive water jet machining, Springer, 1998
- (2) S. Shimizu, Development of abrasive water suspension jet, Proc. 2002 Korea-Japan Joint Seminar on Water Jet Technology, 2002, pp.19-26
- (3) H. Haferkamp, H. Louis and G. Meier, Cutting of contaminated material by abrasive water jets under the protection of water shield, Proc. 9<sup>th</sup> International Symposium on Jet Cutting Technology, BHRA, 1988, Paper F1, pp.271-287
- (4) H. Haferkamp, H. Louis, and G. Meier, Deep sea application of abrasive water jets: Feasibilities and limitations, Jet Cutting Technology, Elsevier Applied Science, 1991, pp.513-523
- (5) S. Shimizu, T. Nishiyama, T. Shimura, and T. Omote, Drilling capability of submerged abrasive water suspension jet, Water Jetting, BHR Group, 2002, pp.509-520
- (6) T. N. Hung, H. Louis, D. Peter, and T. Senne, Submerged application of abrasive water suspension jets (AWSJs), Water Jetting, BHR Group, 2004, pp.205-216
- (7) Y. Yamauchi, H. Soyama, T. Ikohagi, R. Oba, and K. Sato, Ambient pressure effects upon impinging erosion resulted by highspeed submerged water-jets, Proc. 4<sup>th</sup> Pacific Rim International Conference on Water Jet Technology, 1995, pp.139-150
- (8) H. Soyama, Y. Yamaguchi, Y. Adachi, K. Sato, T. Shindo, and R. Oba, High-speed observations of the cavitation cloud around a high-speed submerged water jet, JSME International Journal, Series B, Vol. 38, No. 2, 1995, pp.245-251
- (9) Y. Yamauchi, S. Kawano, H. Soyama, K. Sato, Y. Matsudaira, T. Ikohagi, and R. Oba, Formation process of vortex ring cavitation in high-speed submerged water jets, Trans. JSME, Ser. B, Vol. 62, No. 593, 1996, pp.72-78, in Japanese
- (10) S. Shimizu, K. Tanioka, and N. Ikegami, Influence of ambient pressure on erosion properties of high speed cavitating jets, Proc. 5<sup>th</sup> Pacific Rim International Conference on Water Jet Technology, 1998, pp.53-64
- (11) K. Kobayashi, Y. Ito, K. Kaito, and R. Oba, Unsteady behavior of cavity boundary directly related to cavity discharge, Trans. JSME, Ser. B, Vol. 71, No. 703, 2005, pp.804-810, in Japanese
- (12) T. Yahiro and H. Yoshida, On the characteristics of high speed water jet in the liquid and its utilization of injection grouting method, Proc. 2<sup>nd</sup> International Symposium on Jet Cutting Technology, 1974, pp.G4-41-G4-62
- (13) A. Miller, D. Daly, and S. Connors, Reach enhancement of a submerged waterjet using air shrouding, Proc. 9<sup>th</sup> American Waterjet Conference, 1997, pp.347-363
- (14) T. Isobe, Development of underwater cutting methods for steel materials using abrasive-jets, Proc. 13<sup>th</sup> Annual Meetings for Water Jet Technology, WJTSJ, 1998, pp.53-58, in Japanese
- (15) S. Shimizu and T. Nishiyama, A sheathed nozzle for abrasive water suspension jets in submerged environments, Water Jetting, BHR Group, 2004, pp.197-20

**Table 1.** Cavitation numbers

$p_i$ MPa	Cavitation number $\sigma$
100	0.00110
200	0.00055
300	0.00033
380	0.00029

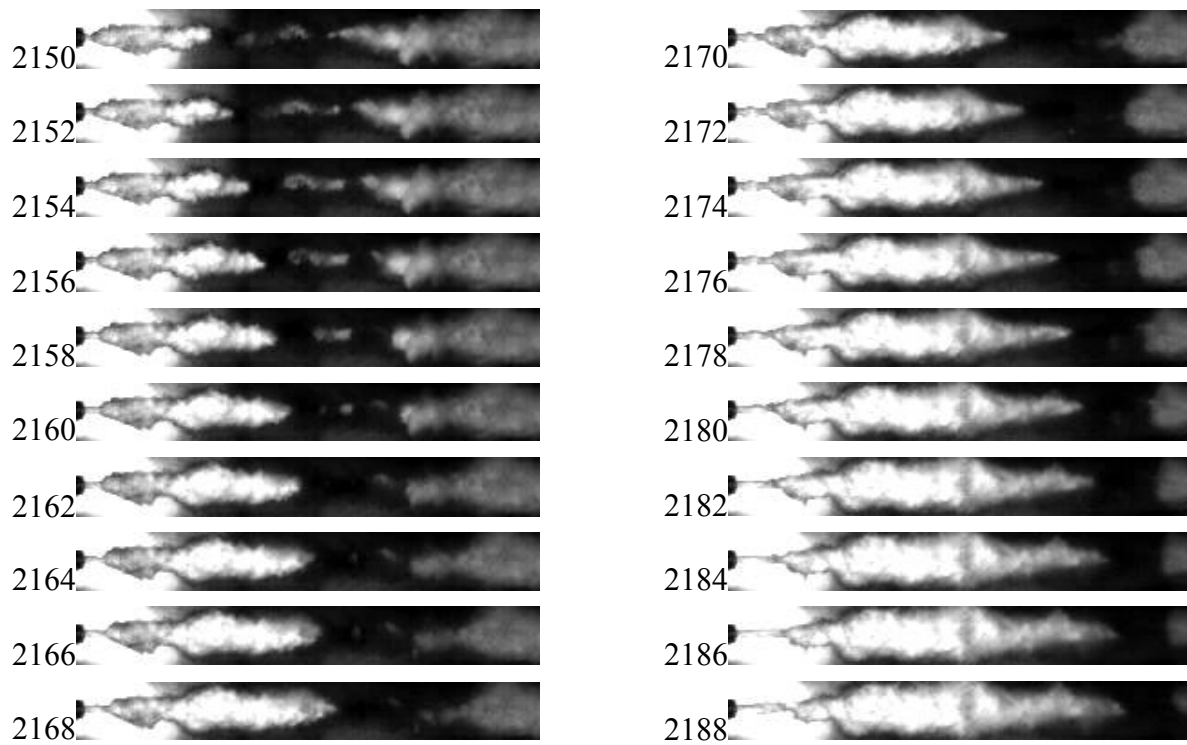


**Figure1.** Series of photographs of submerged jet without air supply at  $p_i = 100$  Mpa

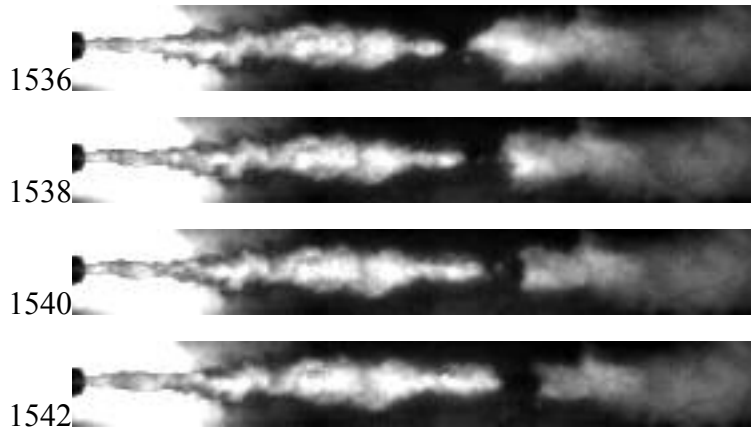


**Figure 2.** Series of photographs of submerged jet without air supply at  $p_i = 100$  MPa

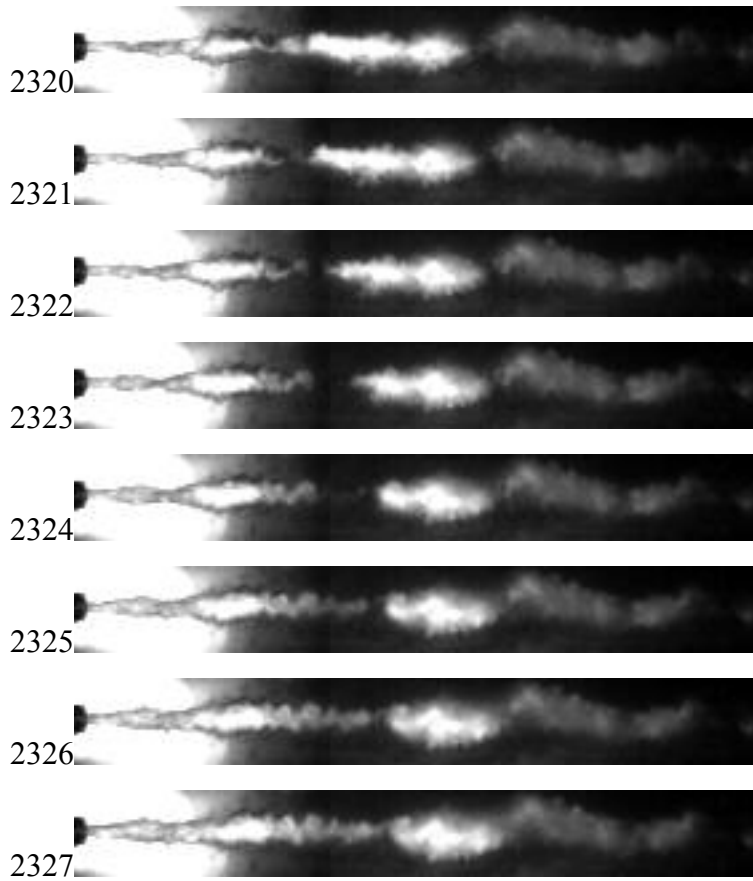


**Figure 3.** Rapid growth of cavitation cloud at  $p_i = 100$  MPa

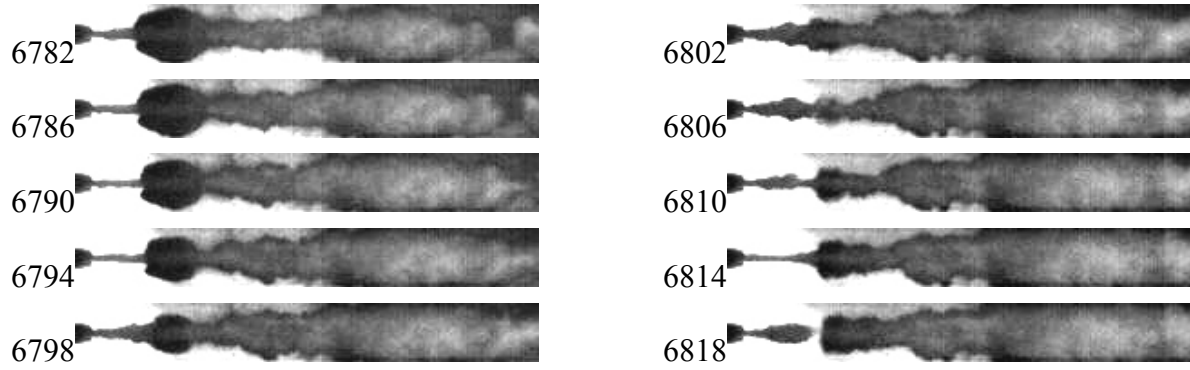


**Figure 4.** Series of photographs of submerged jet without air supply at  $p_i = 300$  MPa

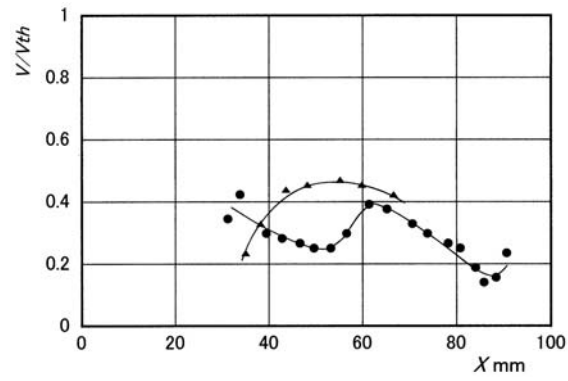


**Figure 5.** Normalized protruding velocity of tongue-like cloud  $V/V_t$  at  $p_i = 100$  MPa

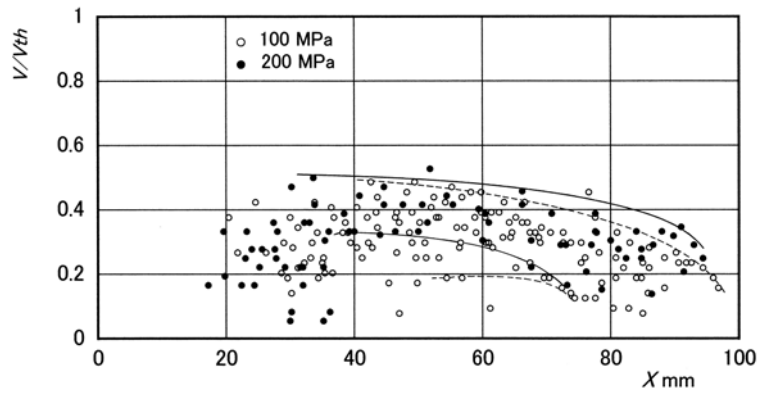


**Figure 6.** Distribution of  $V/V_{th}$  for  $p_i = 100$  and 200 MPa

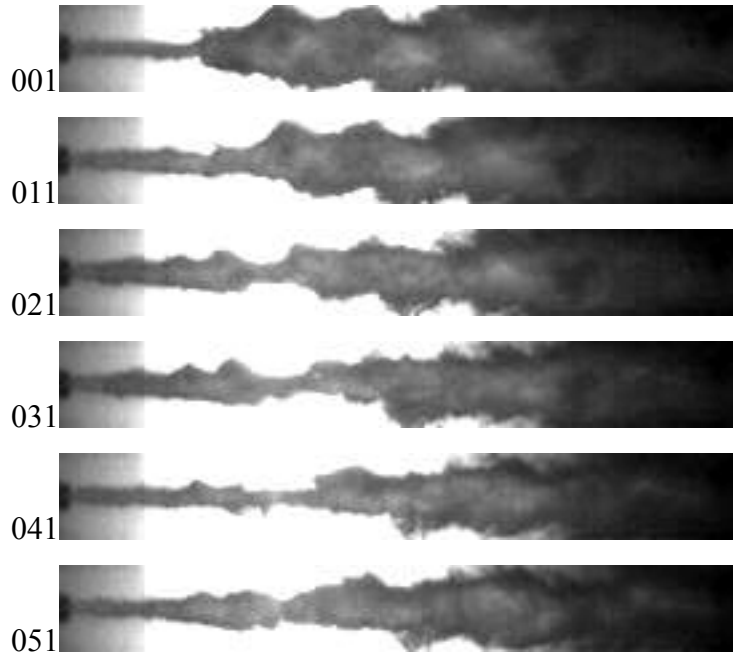


**Figure 7.** Series of photographs of ventilated jet at  $p_i = 300$  MPa and  $Q_{air} = 20$  NL/min

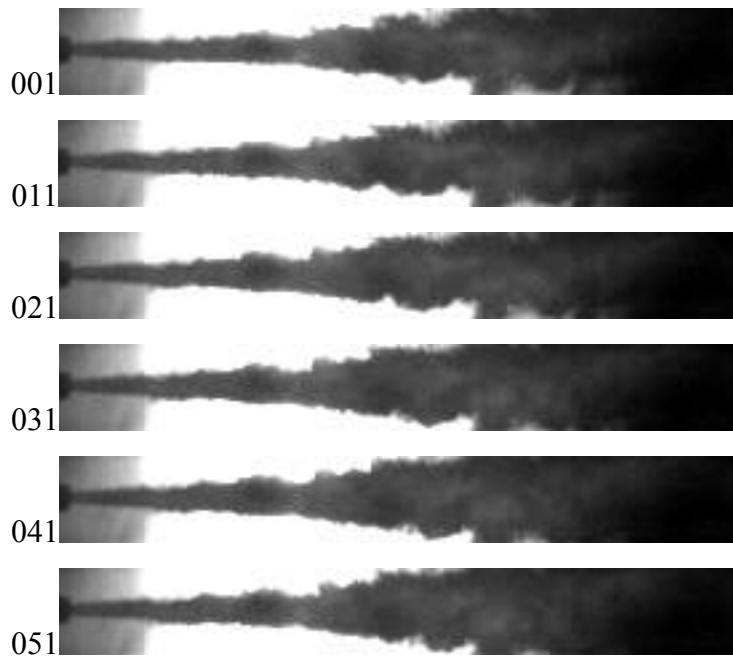


**Figure 8.** Series of photographs of ventilated jet at  $p_i = 300$  MPa and  $Q_{air} = 50$  NL/min

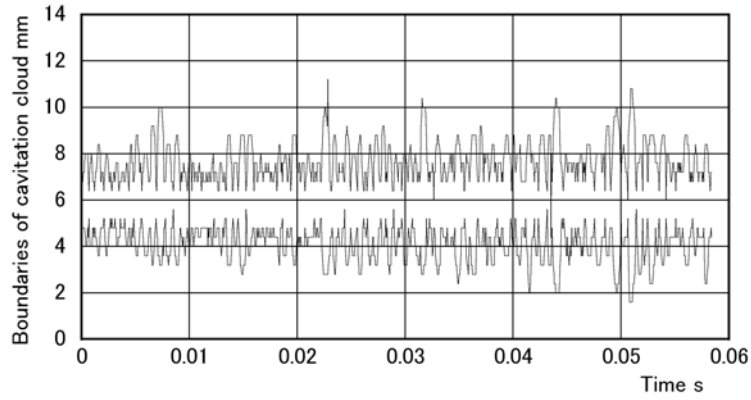


**Figure 9.** Boundaries of cavitation cloud at  $X = 10$  mm  
 ( $p_i = 100$  MPa,  $Q_{air} = 0$  NL/min )

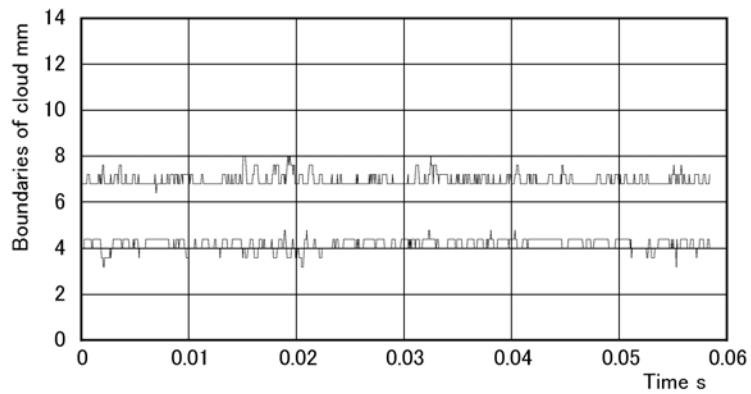


**Figure 10.** Boundaries of ventilated cavity cloud at  $X = 10$  mm  
 ( $p_i = 100$  MPa,  $Q_{air} = 20$  NL/min )

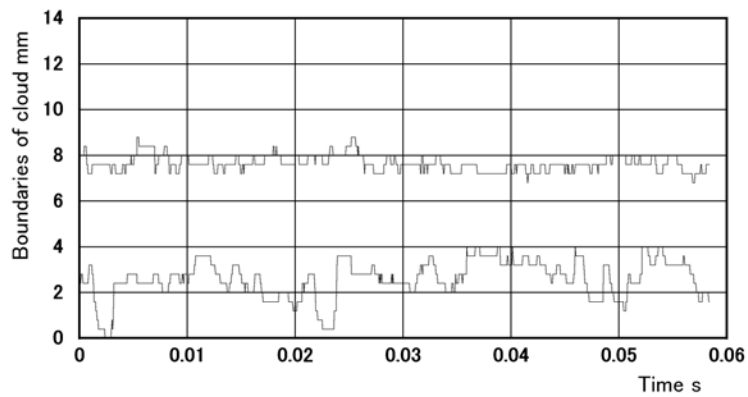


**Figure 11.** Boundaries of ventilated cavity cloud at  $X = 10$  mm  
 ( $p_i = 100$  MPa,  $Q_{air} = 50$  NL/min )

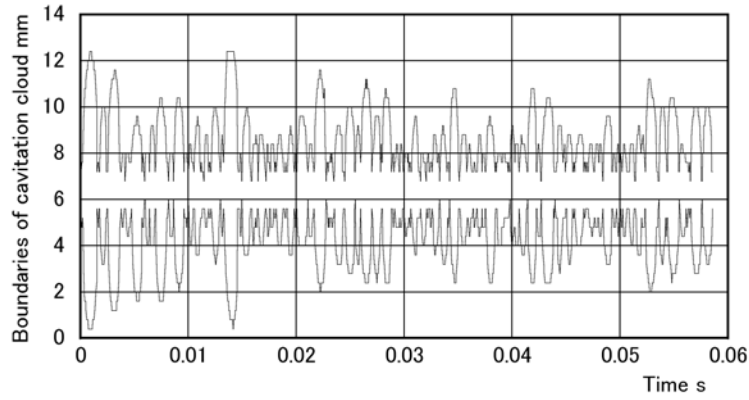


**Figure 12.** Boundaries of cavitation cloud at  $X = 10$  mm  
 ( $p_i = 300$  MPa,  $Q_{air} = 0$  NL/min )

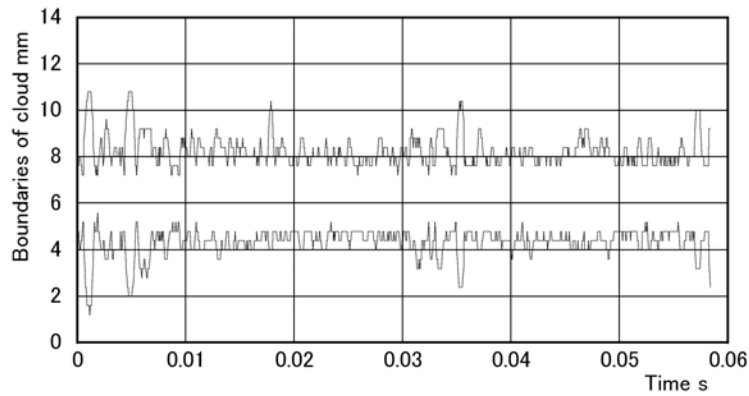


**Figure 13.** Boundaries of ventilated cavity cloud at  $X = 10$  mm  
 ( $p_i = 300$  MPa,  $Q_{air} = 20$  NL/min )

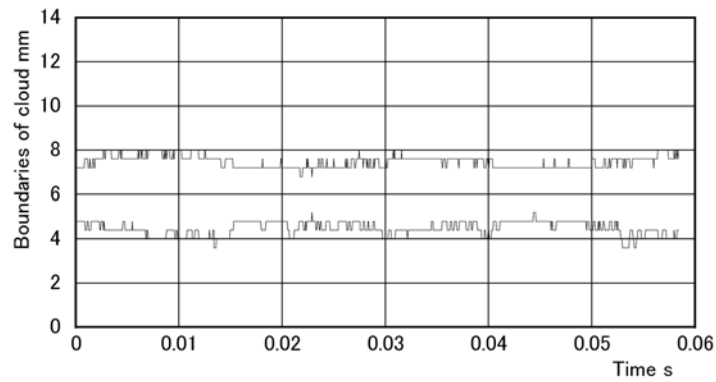


**Figure 14.** Boundaries of ventilated cavity cloud at  $X = 10$  mm  
 ( $p_i = 300$  MPa,  $Q_{air} = 50$  NL/min )

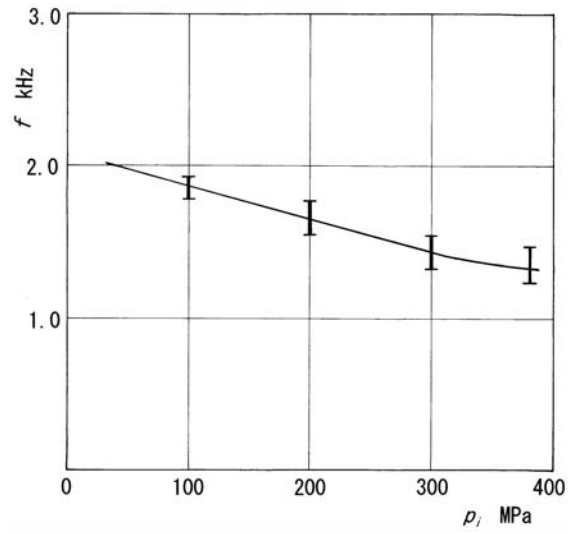


**Figure 15.** Occurrence frequency of vortex ring cavitation versus injection pressure at  $X = 10\text{mm}$

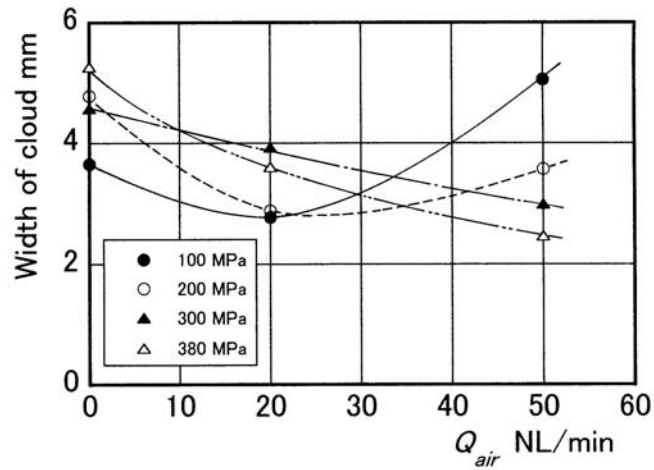


**Figure 16.** Average cloud diameter versus air flow rate

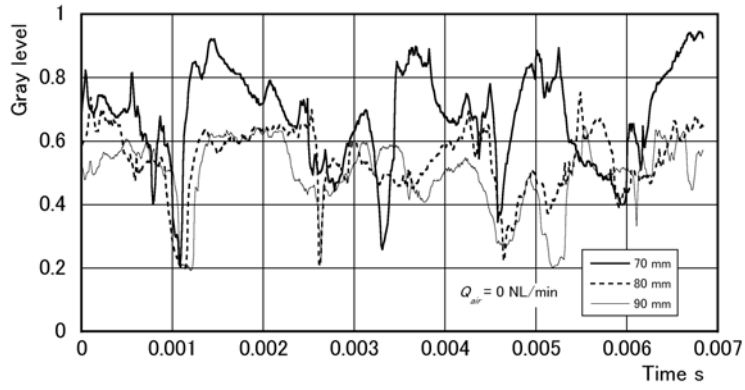


**Figure 17.** Time variations of gray level on the jet axis ( $Q_{air} = 0$  NL/min)

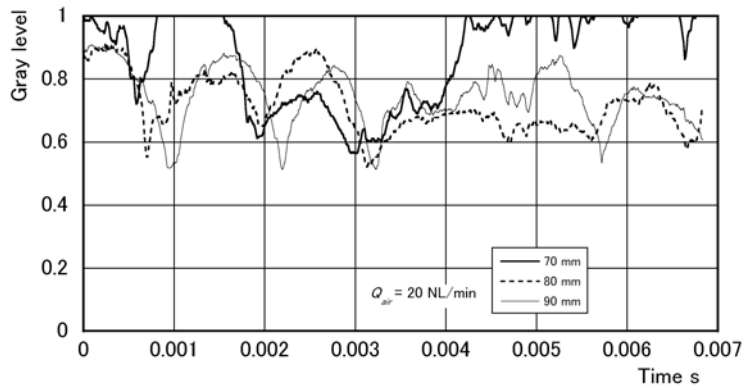


**Figure 18.** Time variations of gray level on the jet axis ( $Q_{air} = 20$  NL/min)

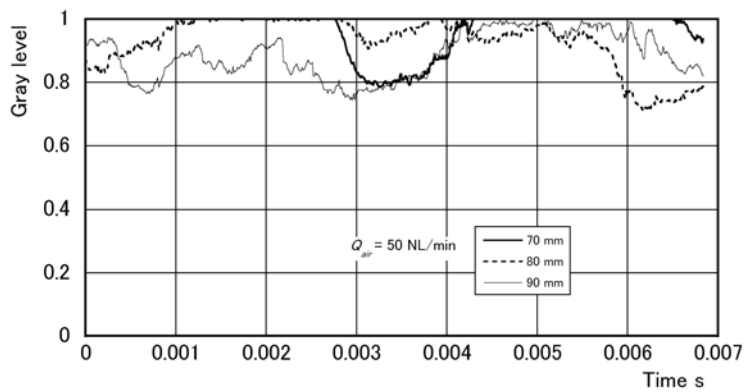


**Figure 19.** Time variations of gray level on the jet axis ( $Q_{air} = 50$  NL/min)